


# Modulation of Q Factor and Fano Lineshape in Ge<sub>2</sub>Sb<sub>2</sub>Te<sub>5</sub>-Based Grating Structure

Qing Liu, Danyang Yao, Yan Liu , Xinyi Liu, Yong Zhang, Genquan Han, *Member, IEEE*, and Yue Hao, *Senior Member, IEEE*

**Abstract**—In this paper, the modulation of the Fano resonance (FR) of dielectric grating has been demonstrated by controlling the crystallization fraction of phase change material film. We analyze the optical characteristics of the grating structure thoroughly by the energy band structure, Q factor, and the electric field distribution of three TE modes. It is verified that the Q factor and the Fano lineshape are related to the thickness of the Ge<sub>2</sub>Sb<sub>2</sub>Te<sub>5</sub> (GST) layer. In addition, by changing the crystallization fraction of the GST layer, non-volatile modulation of the Q factor can be achieved. We also demonstrate that the crystallization fraction of the GST layer affects the Fano lineshape significantly. By changing the crystallization fraction of the GST layer, the non-volatile modulation of Fano lineshape from asymmetric parameter  $q = -1$  to  $q = 1$  can be achieved. These features make this grating structure an excellent optically reconfigurable device in various fields including lasing spaser and biosensing with improved performance.

**Index Terms**—Fano resonance, Ge<sub>2</sub>Sb<sub>2</sub>Te<sub>5</sub>, Q factor, fano lineshape.

## I. INTRODUCTION

**B**OUND states in the continuum (BICs) can achieve perfect confinement when the Q factor is close to infinity, even if their frequencies are within a continuum of leaky modes. Therefore, a high Q factor can be achieved by an optical microcavity that uses the BIC principle [1]. The concept of BICs has been extended to acoustics [2], photonics [3], and electronics [4] since the wave phenomenon can be explained by destructive interference. BICs in photonic systems were first implemented by Marinica *et al.* in 2008 [5]. With the development of nanofabrication technologies, BICs in photonic nanostructures have made great progress, and have been widely used in the fields of sensors

[6], lasers [7], and filters [8]. BICs can be divided into different types according to the different design structures. In an in-plane symmetrical structure, will appear a symmetry-protected BIC at the center of the Brillouin zone (i.e., the  $\Gamma$  point) [9]. When the vertical symmetry of the structure is broken, F-W BICs can emerge from the avoided crossing between modes of opposite parties [10]. And F-W BIC has a wide range of applications in tunable and steerable filters and sensors [11]. Recently, more and more researchers have focused on modulating the Q factor by changing the geometrical parameters of the structure [12]. There are few studies on other ways to modulate the Q factor.

The conclusion that the BIC phenomenon can be produced by Fano resonance (FR) was proposed by S. Weimann *et al.* in 2013 [13]. Therefore, the characteristics of FR will have an important effect on the BIC phenomenon. FR, an electromagnetic interference effect, is caused by the interference between the spectrally broad bright mode strongly coupled with the incident light and the spectrally sharp dark mode with negligible radiation loss [14]. Generally, researchers use symmetry-breaking structures to excite FR. For example, asymmetric split-rings [15], dipole-quadrupole coupled [16], and detuned plasmonic/dielectric resonator-pairs structures [17] have been proven to be used to excite FR. In recent years, dynamically tune the Fano lineshape has aroused great interest among researchers. It has been demonstrated that by tuning the geometrical parameters of the structure, the Fano lineshape can be easily controlled [18], and the tiny disturbance of the structure parameters will lead to great changes in its transmission intensity and frequency spectrum [19]. In addition, by integrating nonlinear materials [20], phase change materials [18], [21], or graphene [22], [23], the Fano lineshape can also be controlled. In efficient nanolasing [24] and biosensing [25], it is necessary to control the spectral positions of both the bright and the dark modes of FR. Therefore, the control of the Fano lineshape has become an increasingly important issue.

Although the Q factor and the Fano lineshape can be controlled by changing the structure parameters, it is difficult to adjust their structure parameters once a structure using traditional materials is fabricated [18], [26], thus their scope of applications is limited. The working performance of the optical system can be greatly improved if the technical parameters or functions of the optical device can be adjusted on site. Therefore, reconfigurable optical devices have become the focus of research in the field of optics in recent years. Optically reconfigurable devices have great application prospects in many fields such as

Manuscript received September 28, 2021; accepted October 5, 2021. Date of publication October 11, 2021; date of current version October 26, 2021. This work was supported by the National Key Research and Development Project under Grant 2018YFB2200500, in part by the National Natural Science Foundation of China under Grants 62004145, 62025402, 62090033, 91964202, 92064003, 61874081, 61851406, and 62004149, and in part by the Major Scientific Research Project of Zhejiang Lab under Grant 2021MD0AC01. (Corresponding authors: Danyang Yao; Yan Liu.)

Qing Liu, Danyang Yao, Yan Liu, Xinyi Liu, Yong Zhang, and Yue Hao are with the State Key Discipline Laboratory of Wide Band Gap Semiconductor Technology, School of Microelectronics, Xidian University, Xi'an 710071, China (e-mail: liuqing6\_6@163.com; dyao@xidian.edu.cn; xdluayan@xidian.edu.cn; 847448333@qq.com; yzhang\_7@126.com; yhao@xidian.edu.cn).

Genquan Han is with the State Key Discipline Laboratory of Wide Band Gap Semiconductor Technology, School of Microelectronics, Xidian University, Xi'an 710071, China, and also with the Research Center for Intelligent Chips, Zhejiang Lab, Hangzhou 311121, China (e-mail: hangenquan@ieec.org).

Digital Object Identifier 10.1109/JPHOT.2021.3119178

optical computing and biomedicine due to their unique functions [27], [28]. Therefore, we consider the utilize of phase change materials (PCMs). The  $\text{Ge}_2\text{Sb}_2\text{Te}_5$  (GST) is an excellent PCM with reconfigurable characteristics. It has a very large refractive index in the infrared range, and the phase change can be thermally [29], optically [30], or electrically [31] induced potentially with an ultrahigh-speed. For example, the PCM transformation occurs in a timescale of nanosecond or even sub-nanosecond [31]. The phase transitions induced by electricity are more suitable to be used on the grating. It is worth noting that GST exhibits distinct optical and electrical properties between its amorphous and crystalline states [32]. By carefully changing the input energy pulse, the reversibility between phase states can be achieved [33]. Besides, this material has the “self-holding” property, consequently, there is no static power consumption to maintain the states [34]. Reconfigurable metamaterials or metasurfaces can be constructed using the large difference in the complex refractive index of the amorphous and the crystalline phases of GST [35]. By changing the state of GST in the mid-infrared (MIR) spectrum, the metamaterial with non-volatile and active tuning characteristics with resonance wavelength shift has been realized [36]. Besides, Phase-change memory (PCM) devices are realized by amorphization- and crystallization-induced changes in the devices’ electrical resistances [37]. The GST material can also be used in tailoring efficient and tunable plasmonic devices [38].

In this paper, we investigate a grating structure composed of silicon and GST layer to realize the modulation of Q factor and the Fano lineshape with different crystallization fractions of the GST layer. The energy band structure, Q factor, and the distribution of the electric field are investigated to analyze the optical characteristics of the grating structure. We also find that the Q factor and the Fano lineshape can be adjusted by changing the thickness of the GST layer. It is verified that the modulation of the Q factor can be achieved by changing the crystallization fraction of the GST layer. In addition, the Fano lineshape is demonstrated to be strongly dependent on the crystallization fraction of the GST layer. This grating structure with the GST layer provides a new reconfigurable choice for various fields, such as lasing spaser and biosensing.

## II. DEVICE STRUCTURE

Fig. 1 shows the 3D schematic of the designed grating structure with periodicity in the  $x$ -direction and infinity along the  $z$ -direction. The main part of this structure is a Si grating, the grating ridges are covered by a thin GST film, and they are surrounded by fused silica. The refractive index of Si and fused silica are 3.48 and 1.45, respectively. And the refractive index of GST with different crystallization fractions varies from  $3.98 + 0.024i$  (amorphous) to  $6.49 + 1.05i$  (crystalline). In this structure,  $a$  represents the period in the  $x$ -direction,  $w$ ,  $h$ , and  $t$  represent the width of the grating ridge, the thickness of the grating layer, and the thickness of the GST layer, respectively. These parameters are initialized to  $a = 1000$  nm,  $w = 600$  nm,  $h = 300$  nm, and  $t = 50$  nm. In the finite element method (FEM) simulation, a normal incident plane wave is parallel to the  $z$ -axis

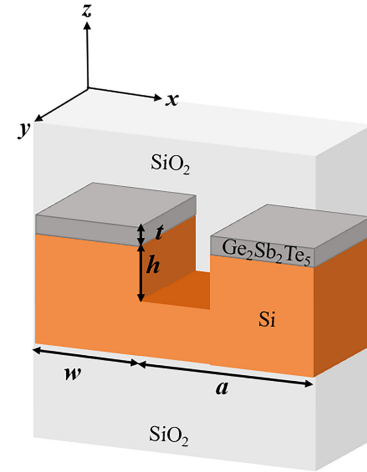


Fig. 1. 3D schematic of the designed grating structure with 1D periodicity in the  $x$ -direction.

with the wave vector  $k$ , and the electric field  $E$  is polarized along the  $y$ -axis. We only investigate the TE-like mode where the incident light propagates in the  $z$ -direction for simplicity. Since the structure is periodic in the  $x$ -direction, only electromagnetic (EM) fields within a one-unit cell need to be simulated. The FEM (COMSOL Multiphysics) simulation methods are adopted to obtain the Q factor and the reflectance of this structure. PML layers are set above and below the fused silica, respectively. In the simulation, the grid size is set to 100 nm. The eigenfrequency module is used to calculate the Q factor.

## III. RESULTS AND DISCUSSION

In this section, we need to calculate the band structure of the grating with the GST layer first. As the Bloch wave vector changes along  $k = (k_x, 0, 0)$ , the band structure and Q factor are calculated using COMSOL Multiphysics. We learn from ref. [39] that the eigenfrequency is expressed as a complex frequency  $f$ , which enables the calculation of the Q factor as

$$Q = \frac{\text{Re}(f)}{2\text{Im}(f)} \quad (1)$$

where the real and imaginary parts of the complex eigenfrequency  $f$  represent the resonance frequency and radiation losses, respectively. Fig. 2(a) illustrates the energy band structure of the designed grating with the amorphous GST layer. We can see that the energy band of the  $\text{TE}_1$  mode is the lowest among the three modes, and the energy band of the  $\text{TE}_2$  mode is very close to the energy band of the  $\text{TE}_3$  mode. The Q factor of these TE modes is calculated with Eq. (1), and the results are shown in Fig. 2(b). It is remarkable in Fig. 2(b) that the Q factor is the largest value at the  $\Gamma$  point in all three modes, especially the  $\text{TE}_3$  mode, the Q factor of it reaches 72753. The three modes located at the  $\Gamma$  point are symmetry-protected BICs generating from the translational symmetry incompatibility between the confined mode and the radiation mode [40], [41]. The even and odd modes of the structure are decoupled when the wave vector is zero, and the symmetry incompatibility mechanism prohibits the

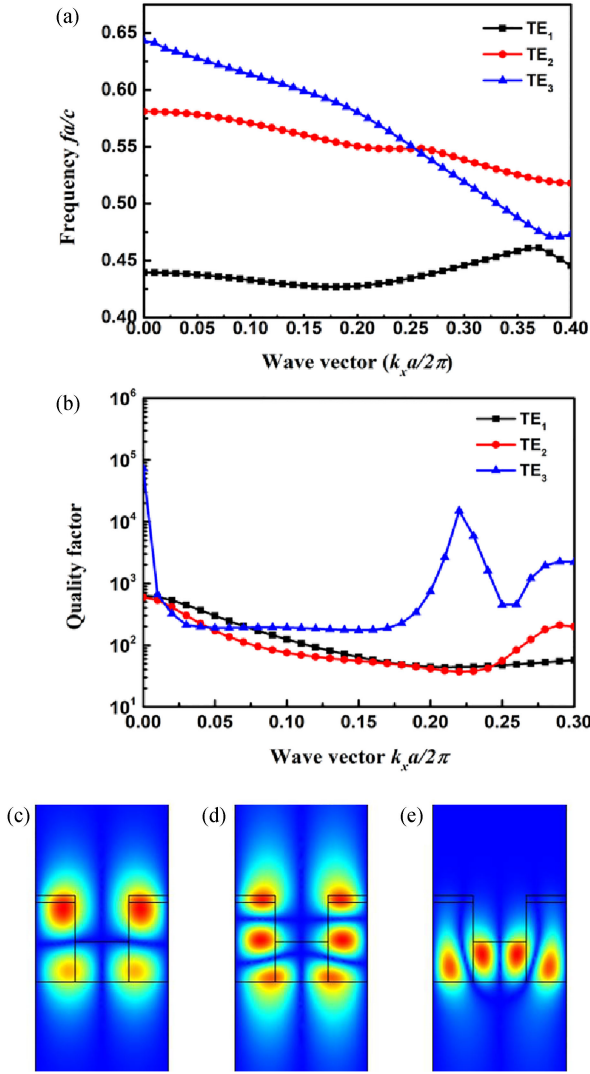


Fig. 2. (a) Calculated band structure of the designed grating structure.  $\text{TE}_1$ ,  $\text{TE}_2$ , and  $\text{TE}_3$  represent the band of different TE-like modes. (b) The Q factor of different TE-like modes of the designed grating structure. (c)–(e) Calculated distribution of  $E_y$  component of three different modes of the symmetry-protected BICs at zero wave vector  $k_x$ .

coupling of modes and the outgoing wave [42]. We can also see from Fig. 2(b) that the  $\text{TE}_3$  mode has an obvious peak at  $k = 0.22$ , and the Q factor reaches 15063, which is a symmetry-breaking BIC. In the grating structure, since the symmetry in the vertical direction is broken, the odd and even resonances will be coupled into a mixed-mode, thereby avoiding resonance crossing [11]. The asymmetry of the coupling caused by the broken vertical symmetry can be described by the two-channel coupled-mode theory. Fig. 2(c)–(e) display the electric field distributions of the trapped states at the  $\Gamma$  point of different TE modes, which show three localized eigenmodes. As we can see from Fig. 2(c)–(e), the light is completely confined in the grating and they are distributed symmetrically along the translational symmetry of the grating without leaky losses. This is consistent with the idea we mentioned earlier that the Q factor is the largest value at the  $\Gamma$  point. It can also be seen from Fig. 2(c)–(e) that the electric fields of  $\text{TE}_1$  and  $\text{TE}_2$  modes are distributed in the entire

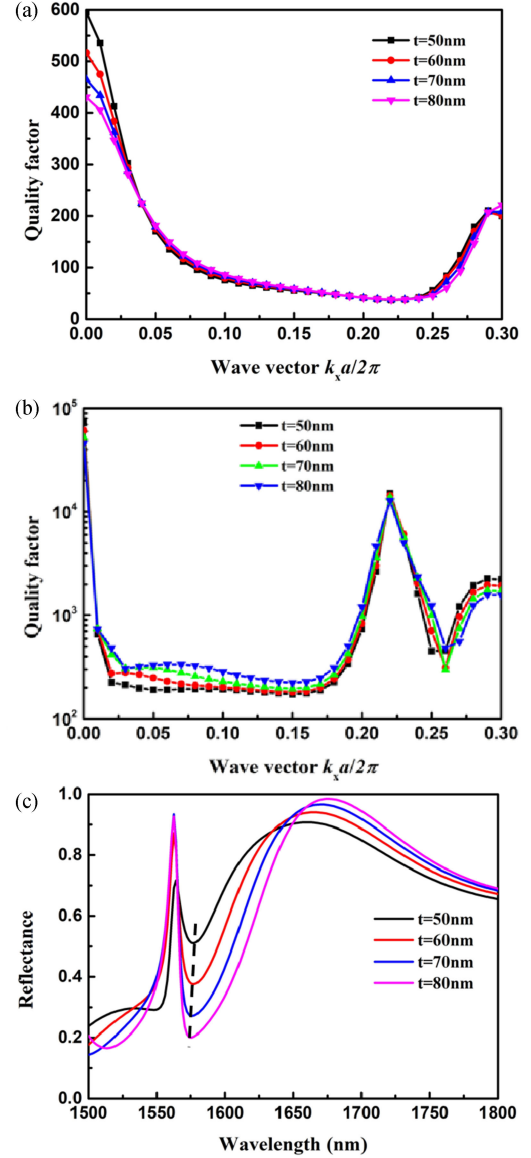


Fig. 3. The Q factor of (a)  $\text{TE}_2$  (b)  $\text{TE}_3$  mode of the designed grating structure with the GST layer, and the thickness of the GST layer changes from 50 nm to 80 nm. (c) The reflection spectra of the grating with the GST layer, and the thickness of the GST layer changes from 50 nm to 80 nm.

grating structure, while the electric field of  $\text{TE}_3$  mode is only distributed in the Si grating part, not in the GST layer. Therefore, the influence of the GST layer on  $\text{TE}_1$  and  $\text{TE}_2$  modes is greater than that on the  $\text{TE}_3$  mode.

Since the energy bands of  $\text{TE}_2$  and  $\text{TE}_3$  modes are very close, the coupling between them will produce Fano resonance, so we will only discuss the influence of the thickness of the GST layer on  $\text{TE}_2$  and  $\text{TE}_3$  modes next. Fig. 3(a) and (b) depict the Q factor of  $\text{TE}_2$  and  $\text{TE}_3$  modes of the grating with different thicknesses of the amorphous GST layer, respectively. It can be seen from Fig. 3(a) and 3(b) that the Q factor of the symmetry-protected BIC at the  $\Gamma$  point of these two modes decreases with the increase of the thickness of the GST layer. In Fig. 3(b), the Q factor of the symmetry-breaking BIC at

$k = 0.22$  also gradually decreases from 15063 to 12883 as the thickness of the GST layer increases. The decrease in the Q factor is due to the large imaginary part of the complex refractive index of GST. Therefore, the thickness of the GST layer influences the Q factor. By changing the thickness of the GST layer, we can obtain the desired Q factor. The reflection spectra of grating with different thicknesses of the amorphous GST layer are shown in Fig. 3(c). We can obtain from Fig. 3(c) that the reflection dips around 1570 nm representing the dark mode and the reflection peaks around 1675 nm representing the bright mode. It can be calculated that as the thickness of the GST layer increases from 50 nm to 80 nm, the Q factor of the dark mode increases from 162 to 184, while the Q factor of the bright mode decreases from 7.67 to 7.03. As shown by the black dashed line in Fig. 3(c), as the thickness of the GST layer increases, the resonant intensity of the dark mode gradually weakens and the resonant wavelength shifts toward a shorter wavelength linearly. However, the resonant intensity of the bright mode gradually increases and the resonant wavelength moves toward a larger wavelength with the increases of the thickness of the GST layer. This means that the coupling of bright mode and dark mode is weakened. We can conclude that by changing the thickness of the GST layer, the Fano lineshape can be flexibly adjusted.

We will discuss the influence of GST layers with different crystallization fractions on TE<sub>2</sub> and TE<sub>3</sub> modes next. The effective dielectric constant of GST with different crystallization fractions can be calculated using the Lorentz relation [26]:

$$\frac{\varepsilon_{eff}(\lambda) - 1}{\varepsilon_{eff}(\lambda) + 2} = m \times \frac{\varepsilon_c(\lambda) - 1}{\varepsilon_c(\lambda) + 2} + (1-m) \frac{\varepsilon_a(\lambda) - 1}{\varepsilon_a(\lambda) + 2} \quad (2)$$

$m$  is the crystallization fraction of the GST layer, ranging from 0 to 1,  $\varepsilon_c(\lambda)$  and  $\varepsilon_a(\lambda)$  are the dielectric constants of GST in the crystalline and amorphous states, respectively. The difference in dielectric constant between the crystalline and amorphous states of GST is relatively large. Amorphous GST can be regarded as a transparent dielectric, while crystalline GST is similar to metal and has a higher optical loss. The tuning range of the crystallization fraction can achieve 10–20 adjustment resolutions on practical occasions. In this paper, the adjustment accuracy of the crystallization fraction of GST is 0.1.

The impact of the crystallization fraction of the GST layer on the Q factor and the corresponding wavelength of the symmetry-protected BIC at the  $\Gamma$  point in TE<sub>2</sub> and TE<sub>3</sub> modes are shown in Fig. 4(a) and (b), respectively. It is clear from Fig. 4(a) and (b) that the Q factor of TE<sub>2</sub> and TE<sub>3</sub> modes at the  $\Gamma$  point gradually decreases with the increase in crystallization fraction. The Q factor of TE<sub>2</sub> mode is decreased from 592 to 22, and this factor of TE<sub>3</sub> mode is reduced from 72753 to 303, as well. The decrease in the Q factor is due to the increase in the crystallization fraction of GST, which leads to the increase in the real and imaginary parts of the refractive index at the same time. The increase of the real part has a positive effect on the Q factor, while the increase of the imaginary part has a negative effect on the Q factor. Obviously, two different mechanisms compete in the Q factor. When the negative effect caused by the imaginary part is superior to the

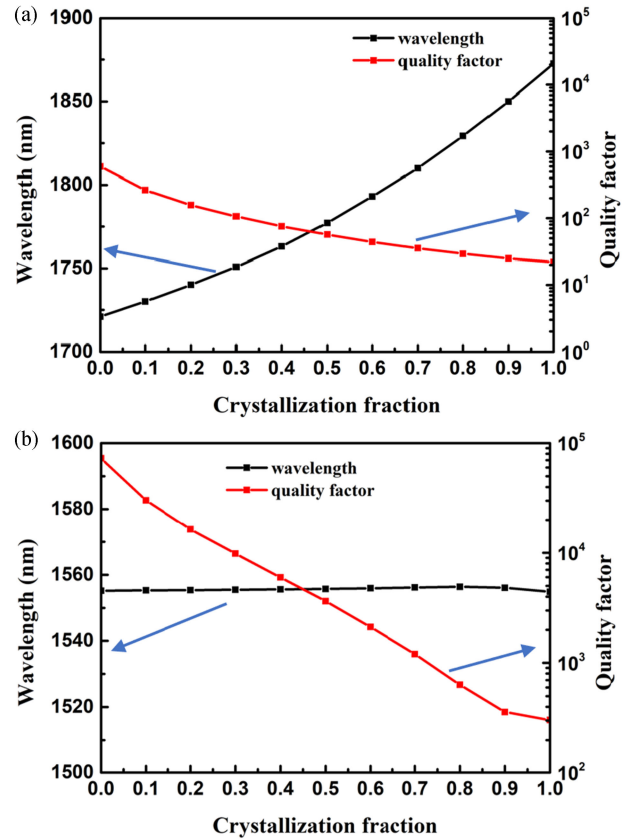


Fig. 4. The quality factor Q and wavelength of the grating at the  $\Gamma$  point in the (a) TE<sub>2</sub> (b) TE<sub>3</sub> mode, as a function of crystallization fraction of GST layer.

positive effect result from the real part, a situation similar to the line of Q factor in Fig. 4(a) and (b) will occur. These results indicate that the crystallization fraction of the GST layer has a great influence on the Q factor. Therefore, we can conclude that the Q factor can be modulated by changing the crystallization fraction of GST. Actually the methods, indicated in equation (1), are different to Ref. [18] that used reflecting spectra to calculate the Q factor. In the reference work, the Q factors are derived by dividing the resonance wavelength by the spectral width between peak and dip wavelengths. To achieve a higher quality factor, an optical microcavity that utilizes the BIC phenomenon should be adopted. Besides, the roughness of the process interface should be minimized to reduce the scattering loss.

We can also obtain from Fig. 4(a) that the wavelength corresponds to the symmetry-protected BIC in TE<sub>2</sub> mode gradually increases from 1720 nm to 1870 nm as the crystallization fraction rises. However, in Fig. 4(b), the wavelength corresponds to the symmetry-protected BIC in TE<sub>3</sub> mode remains unchanged. It is inferred from Fig. 2(d) and (e) that the electric field of TE<sub>2</sub> mode is distributed in the entire grating structure, while the electric field of TE<sub>3</sub> mode is only distributed in the Si grating part, not in the GST layer. Therefore, compared to the TE<sub>3</sub> mode, the wavelength corresponding to the symmetry-protected BIC in the TE<sub>2</sub> mode is more sensitive to the GST layer. These results show that by changing the crystallization fraction of GST, the

wavelength corresponding to the symmetry-protected BIC in  $\text{TE}_2$  mode can be easily adjusted.

To investigate the evolution of reflection spectra of the grating under different crystallization fractions of the GST layer, we calculate the reflectivity as a function of the crystallization fraction of GST and wavelength in Fig. 5(a). In order to clearly see the change of dark mode and bright mode with the crystallization fraction, we redrew the reflection spectra in Fig. 5(b), the black dotted line represents the change of dark mode and the red dotted line represents the change of bright mode. It can be obtained from the calculation that as the crystallization fraction increases, the Q factor of the dark mode decreases from 162.5 to 136.5, and the Q factor of the bright mode decreases from 7.67 to 7.1. As shown by Fig. 5(a) and the black dashed line in Fig. 5(b), the intensity of the dark mode gradually decreases as the crystallization fraction of the GST layer increases. And the resonant wavelength of the dark mode shifts toward a shorter wavelength linearly as the crystallization fraction of the GST layer increases from 0 to 50%. However, the resonant wavelength of the dark mode remains at 1570 nm without shifting as the crystallization fraction of the GST layer rises from 50% to 100%. In addition, it is clear from Fig. 5(a) and the red dashed line in Fig. 5(b) that as the crystallization fraction of the GST layer increases from 0 to 100%, the resonance intensity of the bright mode first increases and then decreases, and the wavelength shift to a larger wavelength. We can obtain from Fig. 5(c) that around 1570 nm, the color gradually varies from green to blue as the crystallization fraction increases. Therefore, the resonance intensity of the dark mode gradually decreases. Besides, the wavelength of the dark mode first shifts to a shorter wavelength and then remains unchanged as the crystallization fraction increases. We can also see that as the crystallization fraction increases, the resonant wavelength of the bright mode gradually shifts to a larger wavelength, and the color first changes to dark orange and then to light orange. Therefore, as the degree of crystallization increases, the resonance wavelength of the bright mode gradually increases, and the resonance intensity first increases and then decreases. These results are consistent with the phenomena in Fig. 5(a) and (b).

Apart from these phenomena, it can be inferred from Fig. 5(a) that the Fano lineshape is asymmetric, which is the property of FR obtained in a specific wavelength region, independent of the crystallization fraction (i.e., phase) of GST. We can conclude that the asymmetric Fano lineshape can be modulated by changing the crystallization fraction of the GST layer. FR exhibits an obvious asymmetric shape and has the following functional form [43]:

$$I \propto \frac{(q\gamma + \omega - \omega_0)^2}{(\omega - \omega_0)^2 + \gamma^2} \quad (3)$$

where  $\gamma$  and  $\omega_0$  are standard parameters, indicating the position and width of the resonance, respectively;  $q$  is the asymmetric parameter of FR, which describes the degree of asymmetry. Next, we will use the asymmetry parameter  $q$  to measure the change of the Fano lineshape caused by the change in the crystallization fraction of the GST layer. In order to study the crystallization fraction of the GST layer on the degree of modulation of the

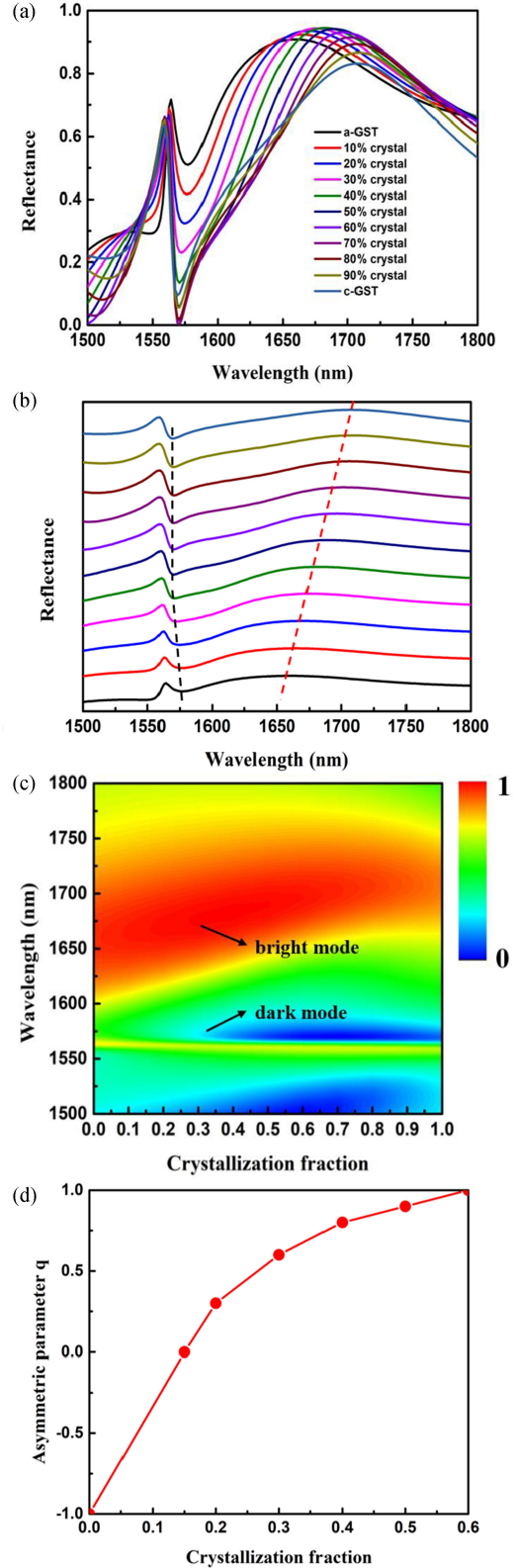


Fig. 5. (a) The reflection spectra of the grating with different crystallization fractions of GST layer. (b) The reflection spectra of the grating with different crystallization fractions of GST layer, the crystallization fraction changes from 0 to 1 (from down to up), the black dotted line represents the change of dark mode and the red dotted line represents the change of bright mode. (c) Reflection map as a function of wavelength and the crystallization fraction of GST layer. (d) Correspondence between the crystallization fraction of GST layer and the asymmetric parameter  $q$ .

Fano lineshape, we plot the corresponding relationship between the crystallization fraction of the GST layer and the asymmetric parameter  $q$  in Fig. 5(d). It can be seen from Fig. 5(d) that as the crystallization fraction of the GST layer increases from 0 to 0.6, the asymmetric parameter  $q$  increases from  $-1$  to  $1$ . Moreover, we can also obtain from Fig. 5(d) that when the crystalline fraction of the GST layer is small, the asymmetry parameter  $q$  increases relatively quickly. However, when the crystalline fraction of the GST layer becomes larger, the asymmetry parameter  $q$  increases slowly. These results indicate that by changing the crystallization fraction of the GST layer, the Fano lineshape can be modulated from  $q = -1$  to  $q = 1$ . That is, the modulation of the Fano lineshape caused by changing the crystallization fraction of the GST layer is consistent with that caused by changing the asymmetric parameter  $q$ . And this modulation is non-volatile due to the non-volatile property of GST material.

#### IV. CONCLUSION

In this work, a grating structure with the GST layer is investigated to achieve the modulation of the Q factor and the Fano lineshape. And optical characteristics of this grating structure are thoroughly analyzed by the band structure, Q factor, and the distribution of the electric field. The Q factor and the Fano lineshape can be adjusted by changing the thickness of the GST layer. Besides, we find that the crystallization fraction of the GST layer has a great influence on the Q factor. Apart from what has been mentioned above, by changing the crystallization fraction of the GST layer, the Fano lineshape will change greatly, and this change is non-volatile. These results provide some useful guidance for the application of optically reconfigurable devices.

#### REFERENCES

- [1] X. W. Gao, B. Zhen, M. Soljacic, H. Chen, and C. W. Hsu, "Bound states in the continuum in fiber Bragg gratings," *ACS Photon.*, vol. 6, pp. 2996–3002, 2019.
- [2] A. A. Lyapina, D. N. Maksimov, A. S. Pilipchuk, and A. F. Sadreev, "Bound states in the continuum in open acoustic resonators," *J. Fluid Mech.*, vol. 780, pp. 370–387, 2015.
- [3] M. I. Molina, A. E. Miroschnichenko, and Y. S. Kivshar, "Surface bound states in the continuum," *Phys. Rev. Lett.*, vol. 108, no. 7, 2012, Art. no. 070401.
- [4] C. Álvarez, F. Domínguez-Adame, P. A. Orellana, and E. Díaz, "Impact of electron–vibron interaction on the bound states in the continuum," *Phys. Lett. A*, vol. 379, no. 14–15, pp. 1062–1066, 2015.
- [5] D. C. Marinica, A. G. Borisov, and S. V. Shabanov, "Bound states in the continuum in photonics," *Phys. Rev. Lett.*, vol. 100, no. 18, 2008, Art. no. 183902.
- [6] C. Z. Fang *et al.*, "Germanium-tin alloys: Applications for optoelectronics in mid-infrared spectra," *Opto-Electron. Adv.*, vol. 1, no. 3, 2018, Art. no. 180004.
- [7] A. Kodigala, T. Lepetit, Q. Gu, B. Bahari, Y. Fainman, and B. Kante, "Lasing action from photonic bound states in continuum," *Nature*, vol. 541, no. 7636, pp. 196–199, 2017.
- [8] J. M. Foley, S. M. Young, and J. D. Phillips, "Symmetry-protected mode coupling near normal incidence for narrow-band transmission filtering in a dielectric grating," *Phys. Rev. B*, vol. 89, no. 16, 2014, Art. no. 165111.
- [9] C. W. Hsu, B. Zhen, A. D. Stone, J. D. Joannopoulos, and M. Soljacic, "Bound states in the continuum," *Nat. Rev. Mater.*, vol. 1, no. 9, 2016, Art. no. 16048.
- [10] I. A. Shaimaa, M. S. Vladimir, B. Alexandra, and V. K. Alexander, "Formation of bound states in the continuum in hybrid plasmonic-photonic systems," *Phys. Rev. Lett.*, vol. 121, no. 25, 2018, Art. no. 253901.
- [11] R. Mermet-Lyauoz, F. Dubois, and N. V. Hoang, "Realization of bound state in the continuum induced by vertical symmetry breaking in photonic lattice," 2019, *arXiv:1905.03868*.
- [12] E. N. Bulgakov, D. N. Maksimov, P. N. Semina, and S. A. Skorobogatov, "Propagating bound states in the continuum in dielectric gratings," *J. Opt. Soc. Amer. B*, vol. 35, no. 6, pp. 1218–1222, 2018.
- [13] S. Weimann, *et al.*, "Compact surface fano states embedded in the continuum of waveguide arrays," *Phys. Rev. Lett.*, vol. 111, no. 24, 2013, Art. no. 240403.
- [14] B. Luk'yanchuk, *et al.*, "The fano resonance in plasmonic nanostructures and metamaterials," *Nat. Mater.*, vol. 9, no. 9, 2010, Art. no. 707.
- [15] Y. K. Srivastava, *et al.*, "Ultra-high-Q fano resonances in terahertz metasurfaces: Strong influence of metallic conductivity at extremely low asymmetry," *Adv. Opt. Mater.*, vol. 4, no. 3, pp. 457–463, 2016.
- [16] N. Arju, T. Ma, A. Khanikaev, D. Purtseladze, and G. Shvets, "Optical realization of double-continuum fano interference and coherent control in plasmonic metasurfaces," *Phys. Rev. Lett.*, vol. 114, no. 23, 2015, Art. no. 237403.
- [17] J. Yan *et al.*, "Directional fano resonance in a silicon nanosphere dimer," *ACS Nano*, vol. 9, no. 3, pp. 2968–2980, 2015.
- [18] X. Zou, G. Zheng, Y. Chen, F. Xian, and L. Xu, "Actively tunable mid-infrared fano resonance in Ge<sub>2</sub>Sb<sub>2</sub>Te<sub>5</sub>-based grating structures," *Opt. Mater.*, vol. 88, pp. 54–59, 2019.
- [19] B. Ruan *et al.*, "Fano resonance in double waveguides with graphene for ultrasensitive biosensor," *Opt. Exp.*, vol. 26, no. 13, pp. 16884–16892, 2018.
- [20] Y. Zhu, X. Hu, Y. Huang, H. Yang, and Q. Gong, "Fast and low-power all-optical tunable Fano resonance in plasmonic microstructures," *Adv. Opt. Mater.*, vol. 1, no. 1, pp. 61–67, 2013.
- [21] T. Cao, C. Wei, R. E. Simpson, L. Zhang, and M. J. Cryan, "Fast tuning of double Fano resonance using a phase-change metamaterial under low power intensity," *Sci. Rep.*, vol. 4, no. 1, 2014, Art. no. 4463.
- [22] C. Zeng, Y. Cui, and X. Liu, "Tunable multiple phase-coupled plasmon-induced transparencies in graphene metamaterials," *Opt. Exp.*, vol. 23, no. 23, pp. 545–551, 2015.
- [23] N. K. Emami, T.-F. Chung, A. V. Kildishev, V. M. Shalaev, Y. P. Chen, and A. Boltasseva, "Electrical modulation of fano resonance in plasmonic nanostructures using graphene," *Nano Lett.*, vol. 14, no. 1, pp. 78–82, 2014.
- [24] N. I. Zheludev, S. L. Prosvirnin, N. Papisimakis, and V. A. Fedotov, "Lasing spaser," *Nat. Photon.*, vol. 2, no. 6, pp. 351–354, 2008.
- [25] C. Wu *et al.*, "Fano-resonant asymmetric metamaterials for ultrasensitive spectroscopy and identification of molecular monolayers," *Nat. Mater.*, vol. 11, no. 1, pp. 69–75, 2012.
- [26] C. H. Chu *et al.*, "Active dielectric metasurface based on phase-change medium," *Laser Photon. Rev.*, vol. 10, no. 6, 2016, Art. no. 1600106.
- [27] T. Zhang, S. Mei, Q. Wang, H. Liu, C. T. Lim, and J. Teng, "Reconfigurable optical manipulation by phase change material waveguides," *Nanoscale*, vol. 9, no. 20, pp. 6895–6900, 2017.
- [28] K. Dong *et al.*, "A lithography-free and field-programmable photonic metacanvas," *Adv. Mater.*, vol. 30, no. 5, 2018, Art. no. 1703878.
- [29] H. F. Hamann, M. O'Boyle, Y. C. Martin, M. Rooks, and H. K. Wickramasinghe, "Ultra-high-density phase-change storage and memory," *Nat. Mater.*, vol. 5, no. 5, pp. 383–387, 2006.
- [30] C. M. Chang, C. H. Chu, M. L. Tseng, H.-P. Chiang, M. Mansuripur, and D. P. Tsai, "Local electrical characterization of laser-recorded phase-change marks on amorphous Ge<sub>2</sub>Sb<sub>2</sub>Te<sub>5</sub> thin films," *Opt. Exp.*, vol. 19, no. 10, pp. 9492–9504, 2011.
- [31] D. Loke *et al.*, "Breaking the speed limits of phase-change memory," *Science*, vol. 336, no. 6088, pp. 1566–1569, 2012.
- [32] H. Y. Zhang, L. J. Zhou, J. Xu, L. J. Lu, J. P. Chen, and B. M. A. Rahman, "All-optical non-volatile tuning of an AMZI-coupled ring resonator with GST phase-change material," *Opt. Lett.*, vol. 43, no. 22, pp. 5539–5542, 2018.
- [33] F. Xiong, A. D. Liao, D. Estrada, and E. Pop, "Low-power switching of phase-change materials with carbon nanotube electrodes," *Science*, vol. 332, no. 6029, pp. 568–570, 2011.
- [34] H. Zhang *et al.*, "Ultracompact Si-GST hybrid waveguides for nonvolatile light wave manipulation," *IEEE Photon. J.*, vol. 10, no. 1, pp. 1–10, Feb. 2018.
- [35] Y. Qu, Q. Li, L. Cai, and M. Qiu, "Polarization switching of thermal emissions based on plasmonic structures incorporating phase-changing material Ge<sub>2</sub>Sb<sub>2</sub>Te<sub>5</sub>," *Opt. Mater. Exp.*, vol. 8, no. 8, pp. 2312–2320, 2018.

- [36] Y. Qu, Q. Li, K. Du, L. Cai, J. Lu, and M. Qiu, "Dynamic thermal emission control based on ultrathin plasmonic metamaterials including phase-changing material GST," *Laser Photon. Rev.*, vol. 11, no. 5, 2017, Art. no. 1700091.
- [37] G. Bakan *et al.*, "Extracting the temperature distribution on a phase-change memory cell during crystallization," *J. Appl. Phys.*, vol. 120, no. 16, 2016, Art. no. 164504.
- [38] B. Gerislioglu, G. Bakan, R. Ahuja, J. Adam, Y.K. Mishra, and A. Ahmadi-vand, "The role of  $\text{Ge}_2\text{Sb}_2\text{Te}_5$  in enhancing the performance of functional plasmonic devices," *Mater. Today Phys.*, vol. 12, 2020, Art. no. 100178.
- [39] Q. Y. Yang, Y. Liu, X. T. Gan, C. Z. Fang, and G. Q. Han, "Nonlinear bound states in the continuum of etchless lithium niobate metasurfaces," *IEEE Photon. J.*, vol. 12, no. 5, Oct. 2020, Art. no. 4601209.
- [40] M. L. Ladrón De Guevara and P. A. Orellana, "Electronic transport through a parallel-coupled triple quantum dot molecule: Fano resonances and bound states in the continuum," *Phys. Rev. B*, vol. 73, no. 20, 2006, Art. no. 205303.
- [41] C. W. Hsu *et al.*, "Observation of trapped light within the radiation continuum," *Nature*, vol. 499, no. 7457, pp. 188–191, 2013.
- [42] J. Lee *et al.*, "Observation and differentiation of unique high-Q optical resonances near zero wave vector in macroscopic photonic crystal slabs," *Phys. Rev. Lett.*, vol. 109, no. 6, 2012, Art. no. 067401.
- [43] B. L. Yanchuk *et al.*, "The fano resonance in plasmonic nanostructures and metamaterials," *Nat. Mater.*, vol. 9, no. 9, pp. 707–715, 2010.